한국정밀공학회지 제 32 권 2 호 pp. 117-125 February 2015 / 117
J. Korean Soc. Precis. Eng., Vol. 32, No. 2, pp. 117-125 http://dx.doi.org/10.7736/KSPE.2015.32.2.117
ISSN 1225-9071(Print), ISSN 2287-8769(Online)

◆ 특집 ◆ 회전 유니트 모델링 기술

복합베어링으로 지지된 스핀들의 동적 해석

Dynamic Analysis of Spindle Supported by Multiple Bearings of Different Types

통반칸[1], 배규현[1], 홍성욱[2,✉]
Van-Canh Tong[1], Gyu-Hyun Bae[1], and Seong-Wook Hong[2,✉]

1 금오공과대학교 기전공학과 대학원 (Graduate School, Department of Mechatronics, Kumoh National Institute of Technology)
2 금오공과대학교 기전공학과 (Department of Mechatronics, Kumoh National Institute of Technology)
✉ Corresponding author: swhong@kumoh.ac.kr, Tel: +82-54-478-7344

Manuscript received: 2014.12.9 / Revised: 2015.1.10 / Accepted: 2015.1.14

This paper presents a dynamic modeling method for the indeterminate spindle-bearing system supported by multiple bearings of different types. A spindle-bearing system supported by ball and cylindrical roller bearings is considered. The de Mul's bearing model is extended for calculating ball and cylindrical roller bearing stiffness matrices with inclusion of centrifugal force and gyroscopic moment. The dependence between spindle shaft reaction forces and bearing stiffness is effectively resolved using an iterative approach. The spindle rotor dynamics is established with the Timoshenko beam theory based finite elements. The spindle reaction forces, bearings stiffness and spindle natural frequencies are obtained with taking into account spindle radial load, ball bearing axial preload and rotational speed effects. The developed method is verified by comparing the simulation results with those from a commercial program.

Key Words: Spindle-bearing system (스핀들 베어링 계), Angular contact ball bearing (각접촉 볼베어링), Cylindrical roller bearing (원통 롤러 베어링), Stiffness matrix (강성행렬), Natural frequency (고유진동수)

1. Introduction

Spindle is an essential part in machine tools because its rotor dynamic characteristics have a great influence on the overall performance of machine tools such as precision machining, service life of tooling and accessories, productivity, etc. Nowadays, combination of different bearing types in a spindle system is prevalent to improve the performance of machine tools. The combined use of ball and cylindrical roller bearings in a spindle shaft is believed to give an enhancement in load carrying capacity and thermal stability.[1]

The finite element model is commonly used in rotor dynamic analysis of spindle-bearing system.[2-4] It has been acknowledged that the finite element technique can provide an accurate modeling of rotor-bearing systems and be applicable to a wide range of complex problems in practical engineering design.[5] In the past, however, the finite element based rotor dynamic model normally adopted the stiffness coefficients of rolling element

bearings as given parameters that were assumed to be constant during operation of spindle system. Recently, many researchers have shown that the bearing coefficients strongly depend on the rotational speed and loading conditions.[6-8] Thus, it is necessary to address the coupling between the bearing and spindle in order to obtain accurate bearing stiffness elements along with the spindle dynamic characteristics.

Several research results have been published regarding the coupling of spindle and bearing system. Jorgensen and Shin[9] analyzed the angular contact bearing stiffness and natural frequencies of the spindle with the radial load applied. In their study, the spindle shaft was discretized into lumped elements with which the influence coefficient method was applied to find the load deflection relationship. This method could be applied only for spindles supported by two bearings or two sets of bearings in which each set of bearings is modeled as a stiffness matrix at a single node. Thus, the accuracy of the model with multiple bearings was improper, as well as the model was confined to spindles supported by two sets of bearings. In addition, the determination of bearing induced moment was not mentioned.

Hong et al.[10] improved the Jorgensen and Shin's model[9] so as to apply for indeterminate spindle-bearing systems supported by more than 2 bearings. A new iterative process was proposed to derive reaction forces and bearing stiffness based on the static finite element spindle model.

Cao and Altintas[11] outlined a general method for modeling of spindle-angular contact bearing systems. The combination of bearing dynamic characteristics and spindle shaft using finite element method was performed to derive the dynamic equations for spindle-bearing systems, which were then iteratively solved by the Newton Raphson technique. Although their method was verified to be accurate, much computational effort was required to solve non-linear equations simultaneously.

Most of the previous studies attempted to couple bearing stiffness in the spindle shaft based on finite element model. Then the unknowns of the system were obtained using iterative methods. However, few researches are available on the rotor dynamics of spindle with combined multiple bearings of different types under general loading conditions. This is due to the lack of an effective method to model the coupling between shaft and bearings, especially in indeterminate spindle-bearing systems.

This paper extends the earlier work proposed by Hong et al.[10] to develop a new scheme for calculation of bearing stiffness and spindle shaft reaction forces. The most important contribution of this work is modifying the spindle load and deflection formulation using the so-called modified transfer matrix method. The overall computational procedure is in the same manner as that in Hong et al.[10] The developed technique is then applied for determining natural frequencies of a spindle assembly supported by angular contact ball and cylindrical roller bearings under radial, axial loadings and rotational speed effects. Finally, the presented model is verified with a commercial program.[12]

2. Ball and roller bearing models

The ball and roller bearing models proposed by de Mul et al.[13] are extended in this study. The ball bearing model takes into account the effects of gyroscopic moment, which is neglected in the de Mul's model. Regarding cylindrical roller bearing, a simplified model is developed by applying a few appropriate modifications from the tapered roller bearing model.[8]

In this paper, all the bearing friction and cage forces, thermal expansion of components and lubrication film are neglected. Only the deformation at the contact location between rollers and races is considered, while the bearing races are assumed to remain circular under loading.

2.1 Ball bearing model

A five-degree-of-freedom (DOF) ball bearing model is adopted as shown in Fig. 1(a). The bearing is loaded by external load vector $\{F\}^T = \{F_x, F_y, F_z, M_y, M_z\}$ and displaces by a displacement vector $\{\delta\}^T = \{\delta_x, \delta_y, \delta_z, \gamma_y, \gamma_z\}$. Displacements of inner ring cross-section and contact load are defined, respectively, by

$$\{u\}^T = \{u_r, u_x, \theta\}; \quad \{Q\}^T = \{Q_r, Q_x, T\} \tag{1}$$

where $\{u\}$ depends on global displacement by:

$$\{u\} = [R\Phi]\{\delta\} \tag{2}$$

where the transformation matrix [RΦ] is given as

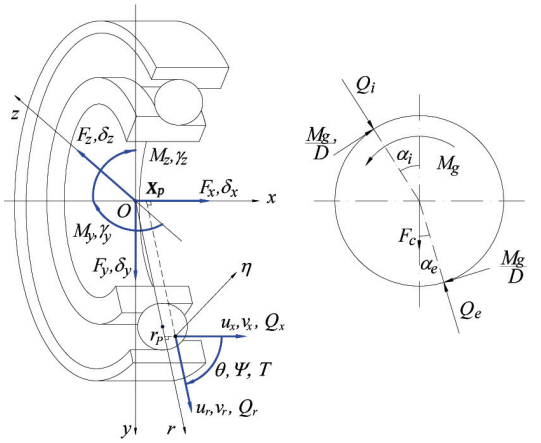

Fig. 1 Ball bearing diagram (a) Coordinate systems and loadings (b) Ball free-body diagram

$$[R\phi]=\begin{bmatrix}\cos\phi & \sin\phi & 0 & -x_p\sin\phi & x_p\cos\phi\\ 0 & 0 & 1 & r_p\sin\phi & r_p\cos\phi\\ 0 & 0 & 0 & -\sin\phi & \cos\phi\end{bmatrix}$$

The ball center displacement is indicated by

$$\{v\}^{\mathrm{T}}=\{v_r,\ v_x\} \tag{3}$$

The ball loading including the centrifugal force and gyroscopic moment is shown in Fig. 1(b). F_c and M_g are the centrifugal force and gyroscopic moment of the ball (see Harris[14]). The contact forces are calculated using the Hertzian theory, as

$$Q_i=K_i\delta_i^{3/2};\quad Q_e=K_e\delta_e^{3/2} \tag{4}$$

The contact deformation can be calculated from the geometric relationship shown in Fig. 2, as

$$\delta_i=l_i-l_{0i};\quad \delta_e=l_e-l_{0e} \tag{5}$$

Having obtained all the loads acting on the ball, one can obtain equilibrium equations at each ball as:

$$\begin{cases}Q_i\cos\alpha_i-Q_e\cos\alpha_e+F_c-\dfrac{M_g}{D}\left(\sin\alpha_i-\sin\alpha_e\right)=0\\ Q_i\sin\alpha_i-Q_e\sin\alpha_e+\dfrac{M_g}{D}\left(\cos\alpha_i-\cos\alpha_e\right)=0\end{cases} \tag{6}$$

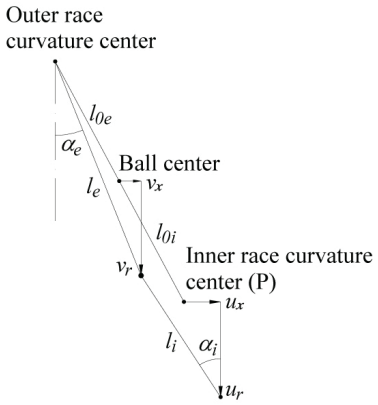

Fig. 2 Ball center, inner and outer race curvature center before and after loading

The Newton-Raphson method is used to solve this system of non-linear equations for the 2 unknowns $\{v_r, v_x\}$. After the ball equations are solved, one can obtain the contact load of inner race as

$$\{Q\}=\begin{Bmatrix}-Q_i\cos\alpha_i+M_g/D\sin\alpha_i\\ -Q_i\sin\alpha_i-M_g/D\cos\alpha_i\\ 0.5M_g/D\end{Bmatrix} \tag{7}$$

Summation of external load and all contact loads acting on the inner ring gives the global equilibrium of bearing as

$$\{F\}+\sum_{j=1}^{n}[R\Phi]^T\{Q\}_j=\{0\} \tag{8}$$

The iterative Newton-Raphson method is also employed for solving the above global equations to obtain the unknowns $\{\delta_x, \delta_y, \delta_z, \gamma_y, \gamma_z\}$. The bearing stiffness matrix can be calculated by referring to de Mul et al.[13] as

$$k=\left[\frac{\partial\{F\}}{\partial\{\delta\}^T}\right]=-\sum_{j=1}^{n}[R\Phi]^T\left[\frac{\partial\{Q\}_j^T}{\partial\{u\}_j}\right][R\Phi] \tag{9}$$

2.2 Roller bearing model

The cylindrical roller bearing can freely move in the axial direction. Thus, the external load and displacement vectors need only 4 DOFs, which can be expressed as, (Fig. 3(a)).

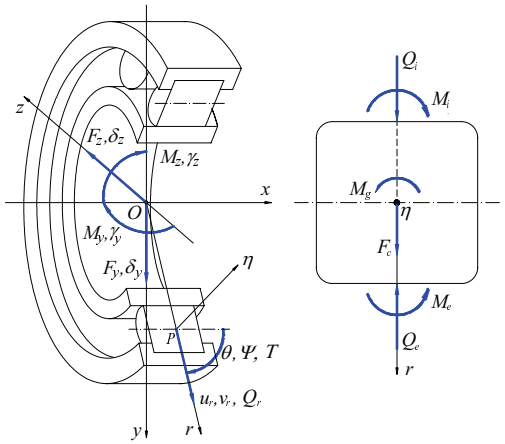

Fig. 3 Cylindrical roller bearing diagram (a) Coordinate systems and loadings (b) Roller free-body diagram

$$\{F\}^{\mathrm{T}} = \{F_y, F_z, M_y, M_z\} \tag{10}$$

$$\{\delta\}^{\mathrm{T}} = \{\delta_y, \delta_z, \gamma_y, \gamma_z\} \tag{11}$$

Due to the fact that the number of DOFs is reduced to 4, modeling procedure for the cylindrical roller bearing is a simplified version of aforementioned ball bearing model. The displacement of inner ring cross-section and contact load can be deduced from Eq. (1) as

$$\{u\}^{\mathrm{T}} = \{u_r, \theta\};\ \{Q\}^{\mathrm{T}} = \{Q_r, T\} \tag{12}$$

From the roller free-body diagram shown in Fig. 3(b), one can obtain the roller equilibrium equation as

$$\begin{cases} Q_i - Q_e + F_c = 0 \\ M_i - M_e - M_g = 0 \end{cases} \tag{13}$$

The roller-races contact loads can be calculated using the slicing technique.[13] The roller contact length is divided into n_s number of slices, and the contact force is then evaluated for each slice as

$$q_k = c\delta_k^{\frac{10}{9}}\Delta l_k;\left(\delta_k > 0\right) \tag{14}$$

The total contact forces and moments become

$$Q = \sum_{k=1}^{n_s} q_k\ ;\quad M = \sum_{k=1}^{n_s} q_k l_k \tag{15}$$

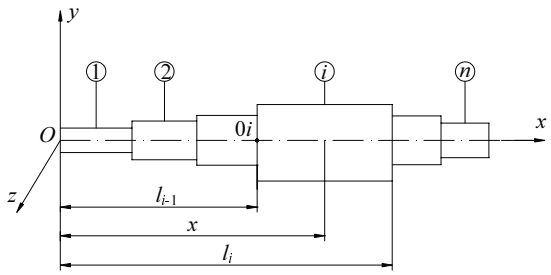

Fig. 4 Spindle shaft with n portions

The inner ring contact load is found as

$$\{Q\} = \begin{Bmatrix} -Q_i \\ -M_i \end{Bmatrix} \tag{16}$$

The global equilibrium equations for the cylindrical roller bearing and the stiffness matrix expressions are similar to Eqs. (8) and (9). It is noted that both roller and global equilibrium equations are non-linear and should be solved using an iterative method such as the Newton-Raphson method.

3. Spindle shaft load-deflection calculation using modified transfer matrix method

A new scheme for calculating spindle shaft deflection is considered here. It is noted that the Euler-Bernoulli beam theory does not give accurate deflection results, particularly in the case of thick beam, since the rotary inertia and shear deformation are not taken into account. Therefore, this section aims to improve the computational accuracy by using the Timoshenko beam theory.

Fig. 4 shows the spindle shaft, which is divided into n portions corresponding to the shaft steps. Considering the elastic deflection $v_i(x)$ at the cross section position x ($l_{i-1} \le x \le l_i$) of portion i whose total length $L_i = l_i - l_{i-1}$. $v_i(x)$ can be expressed in the following form:

$$\begin{aligned} v_i(x) = v_{0i} + v_{0i}^{(1)}(x - l_{i-1}) + v_{0i}^{(2)}\frac{(x-l_{i-1})^2}{2!} \\ + v_{0i}^{(3)}\frac{(x-l_{i-1})^3}{3!} + \ldots + v_{0i}^{(n)}\frac{(x-l_{i-1})^n}{n!} \end{aligned} \tag{17}$$

where v_{0i} denotes the elastic deflection at the left end of portion i. $v_{0i}^{(k)}$ is the k^{th} derivative of v_{0i} with respect to x ($k = 1 \div n$).

Consider a function as below,

$$\Phi_k(x-l_{i-1})=\begin{cases}\dfrac{(x-l_{i-1})^k}{k!};\left(x\ge l_{i-1}\right)\\ 0;\left(0\le x<l_{i-1}\right)\end{cases} \tag{18}$$

Here, function Φ_k possesses the following feature

$$\frac{d\Phi_k}{dx}=\Phi_{k-1} \tag{19}$$

Substituting Eq. (18) into Eq. (17) and then taking derivative the resultant equation with respect to x gives

$$\begin{aligned}
v_i(x)&=v_{0i}\Phi_0+v_{0i}^{(1)}\Phi_1+v_{0i}^{(2)}\Phi_2+v_{0i}^{(3)}\Phi_3+\ldots+v_{0i}^{(n)}\Phi_n\\
v_i^{(1)}(x)&=0+v_{0i}^{(1)}\Phi_0+v_{0i}^{(2)}\Phi_1+v_{0i}^{(3)}\Phi_2+\ldots+v_{0i}^{(n)}\Phi_{n-1}\\
v_i^{(2)}(x)&=0+0+v_{0i}^{(2)}\Phi_0+v_{0i}^{(3)}\Phi_1+\ldots+v_{0i}^{(n)}\Phi_{n-2}\\
v_i^{(3)}(x)&=0+0+0+v_{0i}^{(3)}\Phi_0+\ldots+v_{0i}^{(n)}\Phi_{n-3}
\end{aligned} \tag{20}$$

Eq. (20) can be re-expressed in a matrix form as

$$\begin{Bmatrix}v_i(x)\\ v_i^{(1)}(x)\\ v_i^{(2)}(x)\\ v_i^{(3)}(x)\end{Bmatrix}=\begin{bmatrix}\Phi_0&\Phi_1&\Phi_2&\Phi_3&\ldots&\Phi_n\\ 0&\Phi_0&\Phi_1&\Phi_2&\ldots&\Phi_{n-1}\\ 0&0&\Phi_0&\Phi_1&\ldots&\Phi_{n-2}\\ 0&0&0&\Phi_0&\ldots&\Phi_{n-3}\end{bmatrix}\begin{Bmatrix}v_{0i}\\ v_{0i}^{(1)}\\ v_{0i}^{(2)}\\ v_{0i}^{(3)}\\ \ldots\\ v_{0i}^{(n)}\end{Bmatrix} \tag{21}$$

From the Timoshenko beam theory, the following relationship can be applied

$$\begin{aligned}
v_i^{(1)}(x)&=\frac{dv_i(x)}{dx}=\varphi_i(x)-\frac{Q_i(x)}{\kappa_i G_i A_i}\\
v_i^{(2)}(x)&=\frac{d\varphi_i(x)}{dx}=\frac{M_i(x)}{E_i I_i}\\
v_i^{(3)}(x)&=\frac{1}{E_i I_i}\frac{dM_i(x)}{dx}=\frac{Q_i(x)}{E_i I_i}
\end{aligned} \tag{22}$$

where $\varphi_i(x)$, $M_i(x)$ and $Q_i(x)$ are the shaft angle of deflection, bending moment and shear force at the cross-section x of portion i, respectively. E_i and G_i indicate the elastic and shear moduli of the shaft member. The geometric parameters A_i, I_i and κ_i denote the cross-section area, moment of inertia and shear coefficient, respectively.

In the case of a shaft under concentrated radial load, it is found that

$$v_{0i}^{(1)}=\varphi_{0i}-\frac{Q_{0i}}{\kappa_i G_i A_i};\ v_{0i}^{(2)}=\frac{M_{0i}}{E_i I_i};\ v_{0i}^{(3)}=\frac{Q_{0i}}{E_i I_i} \tag{23}$$

$$v_{0i}^{(k)}=v_i^{(k)}(x)=0;\ \left(k>3\right) \tag{24}$$

where v_{0i}, φ_{0i}, M_{0i} and Q_{0i} represent the elastic deflection, deflection angle, bending moment and shear force at the left end of portion i, respectively. These values are determined by

$$\begin{Bmatrix}v_{0i}\\ \varphi_{0i}\\ M_{0i}\\ Q_{0i}\end{Bmatrix}=\begin{Bmatrix}v_{i-1}\\ \varphi_{i-1}\\ M_{i-1}\\ Q_{i-1}\end{Bmatrix}+\begin{Bmatrix}\Delta v_{0i}\\ \Delta\varphi_{0i}\\ \Delta M_{0i}\\ \Delta Q_{0i}\end{Bmatrix} \tag{25}$$

where $(v_{i-1},\ \varphi_{i-1},\ M_{i-1},\ Q_{i-1})^{\mathrm{T}}$ are the corresponding values at the cross section $x = l_{i-1}$, which have been determined from the previous step using a similar process. $(\Delta v_{i-1},\ \Delta\varphi_{i-1},\ \Delta M_{i-1},\ \Delta Q_{i-1})^{\mathrm{T}}$ indicates the added values for the left end of portion i.

Substituting Eqs. (22)-(25) into Eq. (21), the load-deflection equation for an arbitrary portion of the shaft is obtained as

$$\left\{S_i(x)\right\}=\left[B_i\right]\left(\left\{S_{i-1}\right\}+\left\{\Delta S_{0i}\right\}-\left\{\Delta H_{0i}\right\}\right)+\left\{\Delta H_{0i}\right\} \tag{26}$$

where

$$\left\{S_i(x)\right\}^T=\left\{v_i(x)\quad\varphi_i(x)\quad M_i(x)\quad Q_i(x)\right\} \tag{27}$$

$$\left\{S_{i-1}\right\}^T=\left\{v_{i-1}\quad\varphi_{i-1}\quad M_{i-1}\quad Q_{i-1}\right\} \tag{29}$$

$$\left\{\Delta S_{0i}\right\}^T=\left\{\Delta v_{0i}\quad\Delta\varphi_{0i}\quad\Delta M_{0i}\quad\Delta Q_{0i}\right\} \tag{30}$$

$$\left\{\Delta H_{0i}\right\}^T=\left\{0\quad\frac{\Delta Q_{0i}}{\kappa_i G_i A_i}\quad 0\quad 0\right\} \tag{31}$$

$$\left[B_i\right]=\begin{bmatrix}\Phi_0&\Phi_1&\dfrac{\Phi_2}{E_i I_i}&\dfrac{\Phi_3}{E_i I_i}\\ 0&\Phi_0&\dfrac{\Phi_1}{E_i I_i}&\dfrac{\Phi_2}{E_i I_i}\\ 0&0&\Phi_0&\Phi_1\\ 0&0&0&\Phi_0\end{bmatrix} \tag{32}$$

Using the formula shown in Eq. (26), the governing equations for the first and second portions can be derived. For the first portion, one can get

$$\{S_1(x)\} = [B_1]\left(\{S_0\} + \{\Delta S_{01}\} - \{\Delta H_{01}\}\right) + \{\Delta H_{01}\} \quad (33)$$

Because $\{S_{i-1}\} = \{S_0\} = 0$, Eq. (33) can be further simplified to

$$\{S_1(x)\} = [B_1]\left(\{\Delta S_{01}\} - \{\Delta H_{0i}\}\right) + \{\Delta H_{0i}\} \quad (34)$$

Similarly, the governing equation for the second portion can be written as

$$S_2(x) = [B_2]\left(S_1^* + \Delta S_{02} - \{\Delta H_{02}\}\right) + \{\Delta H_{02}\} \quad (35)$$

It should be noted that

$$\{S_1^*\} = \{S_1(x = l_1)\} \quad (36)$$

The above scheme is used for formulating the relationship of the spindle shaft deflections and reaction forces. It is obvious that the developed scheme could be applicable to a variety of cross-section areas, with different materials and also with general loadings.

4. Natural frequency prediction using finite element model

In this study, the spindle model using Timoshenko beam element as presented in Hong et al.[4] is used for shaft dynamic modeling. The model consists of a spindle shaft and bearings located at nodes. The internal damping is ignored. The equation of motion for a shaft element is described as

$$\begin{bmatrix} m^s & 0 \\ 0 & m^s \end{bmatrix}\begin{Bmatrix} \ddot{y}^s \\ \ddot{z}^s \end{Bmatrix} + \Omega\begin{bmatrix} 0 & g^s \\ -g^s & 0 \end{bmatrix}\begin{Bmatrix} \dot{y}^s \\ \dot{z}^s \end{Bmatrix} + \begin{bmatrix} k^s & 0 \\ 0 & k^s \end{bmatrix}\begin{Bmatrix} y^s \\ z^s \end{Bmatrix} = \begin{Bmatrix} f_y^s \\ f_z^s \end{Bmatrix} \quad (37)$$

In Eq. (37), m^s and g^s denote the (4x4) mass and gyroscopic matrices of shaft element, respectively. $\{y\}^T$ and $\{z\}^T$ indicate (4x1) displacement vectors in *x*-*y* and x-*z* planes.

With neglecting axial displacement of the shaft, the bearing is represented as

$$\begin{bmatrix} k_{xx}^b & k_{xy}^b \\ k_{zy}^b & k_{yy}^b \end{bmatrix}\begin{Bmatrix} y^b \\ z^b \end{Bmatrix} = \begin{Bmatrix} f_x^b \\ f_y^b \end{Bmatrix} \quad (38)$$

where $\{f_y^b \; f_z^b\}^T$ is the bearing force vector. The matrix $k_{ij}^b,(i,j=y,z)$ represents (2x2) bearing stiffness matrix obtained from the bearing model.

Combining the shaft element and bearing equations gives

$$M\ddot{q} + \Omega G\dot{q} + Kq = f(t) \quad (39)$$

The state space form of Eq. (39) can be written as

$$A\dot{h} + Bh = P \quad (40)$$

where

$$A = \begin{bmatrix} M & 0 \\ 0 & M \end{bmatrix};\; B = \begin{bmatrix} 0 & -M \\ K & \Omega G \end{bmatrix};\; h = \begin{Bmatrix} q \\ \dot{q} \end{Bmatrix};\; P = \begin{Bmatrix} 0 \\ f \end{Bmatrix} \quad (41)$$

The eigenvalue problem in association with Eq. (41) can be written as

$$\left(\alpha[A] + [B]\right)\{h\} = \{0\} \quad (42)$$

where α and h denote the eigenvalue and corresponding eigenvector, respectively.

5. Calculation procedure

Because the bearing stiffness depends on shaft reaction forces, and vice-versa, the bearing stiffness and reaction forces should be determined simultaneously.

Fig. 5 shows the block diagram of the entire calculation process. The procedure starts with assuming the radial displacements of bearings. At the first iteration, the induced moments at bearings are assumed to be zero. In the next step, the shaft reaction forces and deflections are determined using the modified transfer matrix method. The output from this step is used to calculate the bearing behavior, e.g., radial displacements, stiffness, induced moments. Then, the iteration process is repeated until the shaft reaction force differences between the current and previous steps are small enough. After the convergence is attained, the spindle natural frequencies are estimated using the dynamic finite element model.

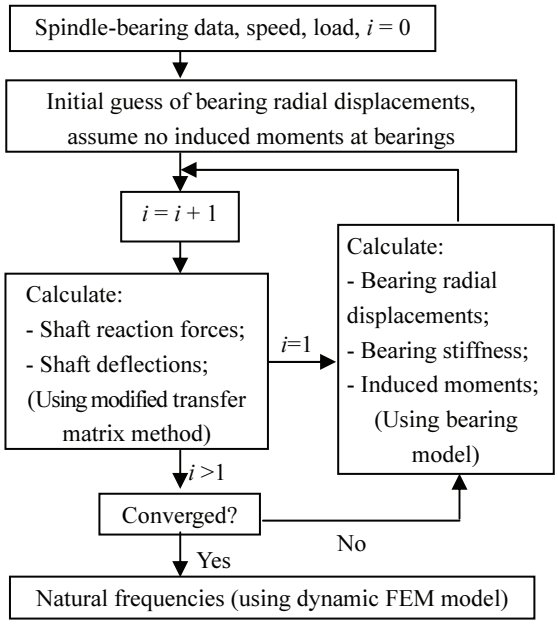

Fig. 5 Calculation block diagram

6. Computational results

In this section, simulation is performed using Matlab to demonstrate the proposed method. Two kinds of bearings such as angular contact bearing B7014 and cylindrical bearing NU1014, are considered throughout the simulation work. The computational results are verified by comparing with those from a commercial program.

6.1 Model verification

The shaft bearing system is loaded with a radial load of F_r = 10,000 N. An axial preload at the middle bearing is F_a = 250 N as shown in Fig. 6. The rotational speed of spindle is n = 5,000 rpm.

Table 1 compares the shaft reaction forces in radial direction from the simulation results using the developed model and the reference program. Table 2 summarizes the induced bearing moments from the developed program and the reference program. Both Tables 1 and 2 exhibit only minor errors between the developed program and the reference program results.

The bearing stiffness coefficients are also compared in Fig. 7. As can be seen in Fig. 7, the maximum difference between the simulation and reference is 1.17% in terms of angular stiffness coefficient $k_{\theta_y\theta_y}$.

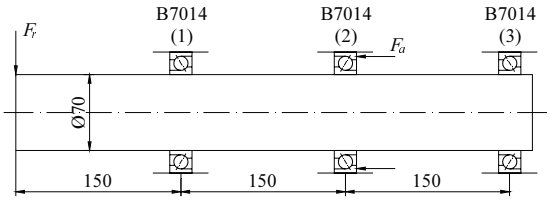

Fig. 6 Simple indeterminate spindle angular contact bearing system

Table 1 Radial reaction forces at bearing locations (N)

Bearings	1	2	3
Reference	15702.55	-750.01	-4952.54
Simulation	1.57E4	-748.241	-4.95E3
Error (%)	0.003	0.236	0.036

Table 2 Induced bearing moment loads (Nmm)

Bearings	1	2	3
Reference	167730	5960	-75420
Simulation	1.68E5	5.99E3	-7.54E4
Error (%)	0.143	0.433	0.005

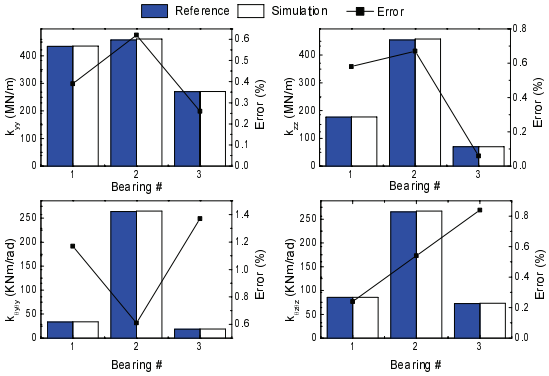

Fig. 7 Bearings stiffness comparison

6.2 Application to an actual spindle system

Fig. 8 shows the investigated spindle-bearing system. The radial load (F_r) is applied at the left end of the spindle to emulate the cutting load during operation. The load F_r is selected from 1,500 to 2,000N, while the rotational speed of system remains constant at n = 5,000rpm.

Figs. (9)-(11) demonstrate the radial stiffness coefficients of cylindrical roller and ball bearings, natural frequencies of spindle-bearing system as a function of applied radial load. The stiffness and frequency

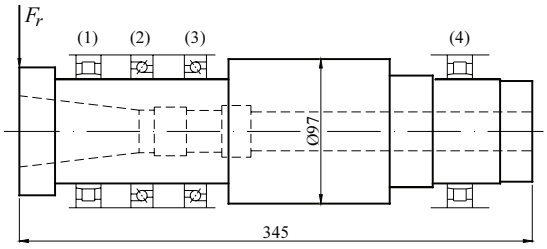

Fig. 8 Investigated spindle-bearing systems

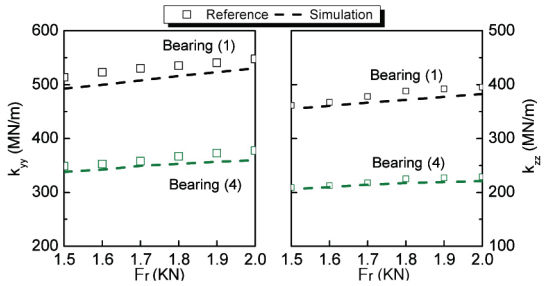

Fig. 9 Radial stiffness of cylindrical roller bearings

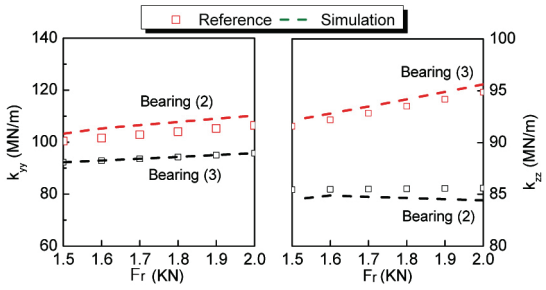

Fig. 10 Radial stiffness of angular contact bearings

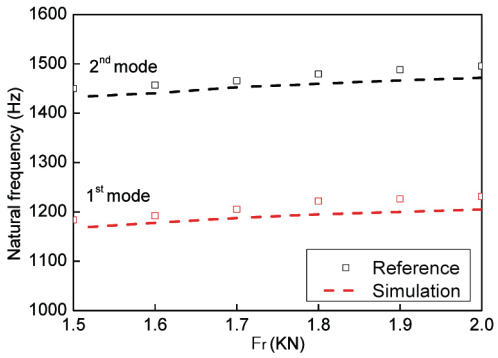

Fig. 11 Spindle-bearing systems natural frequencies

differences between the developed program and reference program are very small.

7. Conclusions

A modeling program for spindle-bearing system has been developed for spindles supported by multiple bearings of different types. An indeterminate spindle-bearing system with angular contact ball bearings and cylindrical roller bearings is investigated to demonstrate the program. The simulation results show that the developed program can well predict the bearing stiffness and spindle dynamic behavior under general loading conditions.

ACKNOWLEDGEMENT

This research was financially supported by the Korea Institute of Machinery and Materials.

REFERENCES

1. SKF Group, “Bearing Arrangements,” http://www.skf.com/group/products/bearings-units-housings/super-precision-bearings/principles/design-considerations/bearing-arrangements/index.html (Accessed DEC. 7, 2014).
2. Nelson, H. D. and McVaugh, J. M., “The Dynamics of Rotor-Bearing Systems using Finite Elements,” J. Manuf. Sci. and Eng., Trans. ASME, Vol. 98, No. 2, pp. 593-600, 1976.
3. Hong, S. W. and Park, J. H., “An Efficient Method for the Unbalance Response Analysis of Rotor-Bearing Systems,” J. Sound & Vibration, Vol. 200, No. 4, pp. 491-504, 1997.
4. Bae, G. H., Lee, C. H., Hwang, J., and Hong, S. W., “Estimation of Axial Displacement in High-Speed Spindle due to Rotational Speed,” J. Korean Soc. Precis. Eng., Vol. 29, No. 6, pp. 671-679, 2012.
5. Chen, L. K. and Ku, D. M., “Finite Element Analysis of Natural Whirl Speeds of Rotating Shafts,” Computers and Structures, Vol. 40, No. 3, pp. 741-747, 1991.
6. Hong, S. W., Choi, C. S., and Lee, C. H., “Effects of Bearing Arrangement on the Dynamic Characteristics of High-Speed Spindle,” J. Korean Soc. Precis. Eng., Vol. 30, No. 8, pp. 854-863, 2013.
7. Noel, D., Ritou, M., Furet, B., and Loch, S. L.,

"Complete Analytical Expression of the Stiffness Matrix of Angular Contact Ball Bearings," J. Tribol. Trans. ASME, Vol. 135, No. 4, Paper No. 041101, 2013.

8. Tong, V. C. and Hong, S. W., "Characteristics of Tapered Roller Bearing Subjected to Combined Radial and Moment Loads," Int. J. Precis. Eng. Manuf.-Green Tech., Vol. 1, No. 4, pp. 323-328, 2014.
9. Jorgensen, B. R. and Shin, Y. C., "Dynamics of Spindle-Bearing Systems at High Speeds including Cutting Load Effects,'' J. Manuf. Sci. Eng., Trans. ASME, Vol. 120, Vol. 2, pp. 387-394, 1998.
10. Hong, S. W., Kang, J. O., and Shin, Y. C., "Dynamic Characteristics of Indeterminate Rotor Systems with Angular Contact Ball Bearings Subject to Axial and Radial Loads," Int. J. Precis. Eng. Manuf., Vol. 3, No. 2, pp. 61-71, 2002.
11. Cao, Y. and Altintas, Y., "A General Method for the Modeling of Spindle-Bearing Systems," J. Mechanical Design, Trans. ASME, Vol. 126, No. 6, pp. 1089-1104, 2005.
12. Schaeffler Technologies, "BEARINX®-online Shaft Calculation," http://www.schaeffler.de/content.schaeffler.de/en/products_services/inafagproducts/calculating/bearinxonline/bearinx_online.jsp/ (Accessed DEC. 05 2014)
13. de Mul, J. M., Vree, J. M., and Maas, D. A., "Equilibrium and Associated Load Distribution in Ball and Roller Bearings Loaded in Five Degrees of Freedom While Neglecting Friction - Part I-II," J. Tribol., Trans. ASME, Vol. 111, pp. 149-155, 1989.
14. Harris, T. A. and Kotzalas, M. N., "Advanced Concept of Bearing Technology," New York, Taylor & Francis, 5th Ed., pp. 68-93, 2007.